# The generation of collimated γ-ray pulse from the interaction between 10 PW laser and a narrow tube target

J. Q. Yu, R. H. Hu, Z. Gong, A. Ting, Z. Najmudin, D. Wu, H. Y. Lu, W. J. Ma, and X. Q. Yan

Citation: Appl. Phys. Lett. **112**, 204103 (2018); doi: 10.1063/1.5030942
View online: https://doi.org/10.1063/1.5030942
View Table of Contents: http://aip.scitation.org/toc/apl/112/20
Published by the American Institute of Physics

# The generation of collimated $\gamma$-ray pulse from the interaction between 10 PW laser and a narrow tube target

J. Q. Yu,[1,a)] R. H. Hu,[1,a)] Z. Gong,[1] A. Ting,[2] Z. Najmudin,[3] D. Wu,[4] H. Y. Lu,[1,5,b)] W. J. Ma,[1,c)] and X. Q. Yan[1,5,6,d)]

[1]*State Key Laboratory of Nuclear Physics and Technology, and Key Laboratory of HEDP of the Ministry of Education, CAPT, Peking University, Beijing 100871, China*
[2]*Institute for Research in Electronics and Applied Physics, University of Maryland, College Park, Maryland 20742, USA*
[3]*The John Adams Institute for Accelerator Science, The Blackett Laboratory, Imperial College London, SW7 2BZ, United Kingdom*
[4]*Shanghai Institute of Optics and Fine Mechanics, Shanghai 201800, China*
[5]*Collaborative Innovation Center of Extreme Optics, Shanxi University, Taiyuan, Shanxi 030006, China*
[6]*Shenzhen Research Institute of Peking University, Shenzhen 518055, China*

(Received 27 March 2018; accepted 20 April 2018; published online 18 May 2018)

A scheme to radiate a highly collimated $\gamma$-ray pulse is proposed through the interaction between an ultra-intense laser pulse and a narrow tube target. The $\gamma$-ray pulse, with high conversion efficiency, can be generated as a result of electron acceleration in a longitudinal electric field. In a Particle-in-Cell simulation with a 10-PW laser, 18% of the laser energy is transferred into the forward $\gamma$-rays in a divergence angle less than 3°. It is also found that such a highly collimated $\gamma$-ray pulse can be produced with a large range of tube diameters and laser intensities. This scheme could be realized in experiment with the coming 10-PW class lasers in the near future. *Published by AIP Publishing.*
https://doi.org/10.1063/1.5030942

The ultra-high laser intensity above $10^{23}$ W/cm$^2$ will be accessible in the next few years with under construction facilities.[1,2] In the interaction between a laser at such an intensity and matter, QED effects[3–6] become significant even when the laser field strength is several orders of magnitude lower than the critical Schwinger field $E_{crit} = 1.3 \times 10^{18}$ Vm$^{-1}$,[7] and most of the laser energy can be transferred into $\gamma$-rays.[8–10] The generation of high conversion efficiency and collimated $\gamma$-ray pulses has attracted particular interest due to potential applications in many fields.[1,5,11–16]

In general, the $\gamma$-ray sources driven by a 10 PW laser have a large divergence[5,8–10,18] of $\sim 30^\circ$. Efforts had been made to enhance collimation of the $\gamma$-rays by employing a micro-structured[17] and narrow tube target.[19,20] In the work of Yi *et al.*,[20] a collimated $x$-ray radiation has been proposed by the laser pulses of relatively low intensity, in which we note that divergence of the $x$-ray increases with the laser normalized amplitude $a_0$. In the narrow tube target under ultra-high laser power, the electron dynamics, which impacts the $\gamma$-ray generation, is affected by the traveling $E_{x.}$[21,22] However, the underlying physics of electron dynamics needs to be further revealed even when the target has been widely applied.[20,22–25]

In this letter, a highly collimated $\gamma$-ray pulse with high conversion efficiency is generated in the interaction between a 10-PW laser pulse and a narrow tube target (NTT). Electrons can experience the acceleration in the longitudinal electric field $E_x$, which significantly improves the electron acceleration and collimation. The $\gamma$-rays are generated near the tube inner boundary where energetic electrons are strongly wiggled by the space charge field $E_{ys}$ and self-generated field $B_{zs}$. In a Particle-in-Cell (PIC) simulation, 18% laser energy is transferred into the forward $\gamma$-rays in a divergence angle less than 3°. These parameters indicate a high brilliance which is two orders of magnitude higher than that of the reported $\gamma$-rays.[5,9,10,17,19,26,27] The effects of the tube diameter and laser intensity are also investigated, and the results show that this scheme works well to produce highly collimated $\gamma$-ray pulses in a wide range of parameters.

Here, we present an analytical model of the electron dynamics in laser fields inside a tube target. The components of linearly polarized Gaussian profiled laser fields[21,22] are the transverse electric field $E_{yL} = v_\phi a_0 \sin\phi$, magnetic field $B_{zL} = a_0 \sin\phi$, and $E_{xL} = \rho a_0 \cos\phi$, where $a_0$ is the amplitude of vector potential $a_y = a_0 \cos(\phi)$, $\phi = v_\phi t - x$ is the laser phase, $v_\phi$ is the phase velocity, and $\rho$ is the ratio of maximum $E_{xL}$ over $a_0$. $E$, $B$, $t$, $x$, $p$, and $a$ are in SI units and normalized by $m_e\omega_l c/e$, $m_e\omega_l/e$, $\omega_l$, $\omega_l/c$, $m_{ec}$, and $m_e c/e$, where $\omega_l$ is the laser frequency, $c$ is the light speed in vacuum, and $m_e$ is the electron mass at rest. The Relativistic Newton-Lorentz equation governing electron motion can be analytically solved. For electrons initially at rest, the transverse momentum is

$$p_y = a_y(\phi) - a_y(\phi_0) = a_0(\cos\phi - \cos\phi_0), \tag{1}$$

and the longitudinal momentum is

$$p_x = \frac{\sqrt{\xi^2 + (v_\phi^2 - 1)(1 + p_y^2)} - v_\phi \xi}{v_\phi^2 - 1}, \tag{2}$$

where $\phi_0$ is the initial phase, $\xi = 1 + \rho a_0 v_\phi(\sin\phi - \sin\phi_0)$.

[a)]J. Q. Yu and R. H. Hu contributed equally to this work.
[b)]Electronic mail: hylu@pku.edu.cn
[c)]Electronic mail: wenjun.ma@pku.edu.cn
[d)]Electronic mail: x.yan@pku.edu.cn

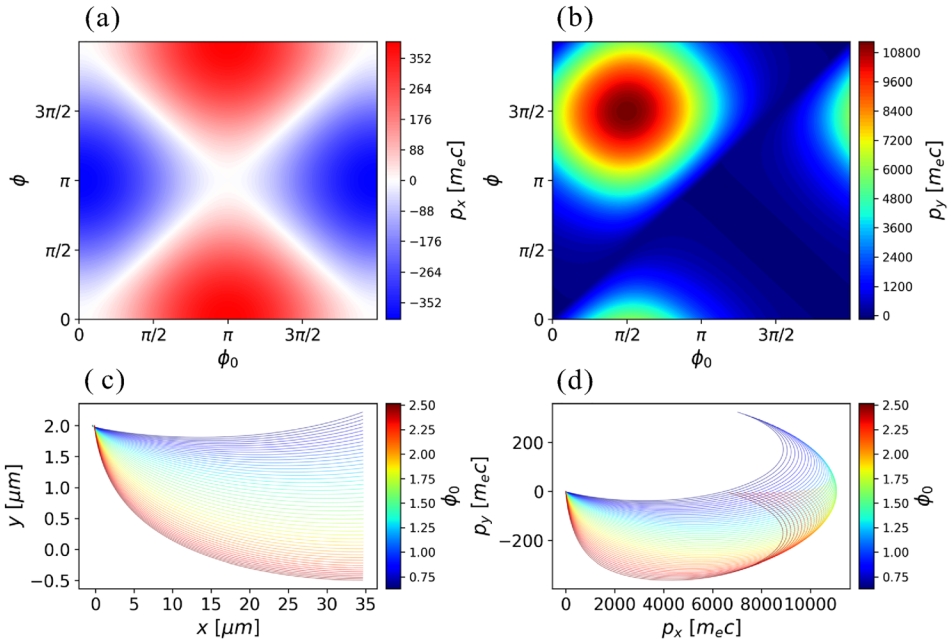


FIG. 1. The numerical results for the electrons initially located at the top side of the tube ($y>0$): (a) $p_y$ as a function of $\phi$ and $\phi_0$, (b) $p_x$ as a function of $\phi$ and $\phi_0$, (c) numerical results of trajectories, and (d) $p_x - p_y$ phase space trajectories of electrons with different $\phi_0$ values. In all the subplots, we assumed $a_0 = 200$, $v_\phi = 1.014$ which is obtained from 2D-PIC simulation and $\rho = 0.39$ is calculated from the laser profile and the tube radius.

Here, we discuss the behaviors of the electrons initially located at the top side of the tube ($y>0$) as an example. Figures 1(a) and 1(b) depict $p_y$ and $p_x$ at different $\phi$ values for different $\phi_0$ values according to Eqs. (1) and (2). In the phase space ($\phi_0$, $\phi$), an electron starts with $\phi = \phi_0$ and $\phi$ increases due to $d\phi/dt = v_\phi - v_x > 0$. The electrons are pulled out of the tube wall by $E_y$ [Fig. 1(c)] at the beginning. The electrons will slip backward with respect to the laser phase because the electron longitudinal velocity is relatively small compared to the light speed and the laser phase velocity $v_\phi$ is larger inside the tube than in the vacuum.[28,29] Then, the electrons are accelerated longitudinally which can surpass $p_y$ very shortly as $\phi$ reaches $2\pi - \phi_0$ [Fig. 1(a)]. $p_x$ increases to maximum as $\phi$ reaches $3\pi/2$ [Fig. 1(b)]. Hence, $p_y \ll p_x$ and highly collimated electrons can be generated near the phase $2\pi - \phi_0$. Figures 1(c) and 1(d) show that the numerical results of electron trajectories are consistent with the above descriptions. The electrons can be trapped by $E_{xL}$ for $t_{trap} \approx 0.5\lambda_0/(v_\phi - c) = 107$ fs, where $\lambda_0$ is the laser wavelength. It is found that the electron divergence angle $\theta_e = p_y/p_x$ decreases with the increasing $a_0$ for given $\phi_0$ ($0 \sim \pi$) and $\phi$ ($\pi \sim 2\pi$). Better collimation at higher laser intensity is completely different from Ref. 20. The transverse non-uniformity of $E_{xL}$ and $E_{yL}$ can moderately alter the trajectories of electrons, but the physics remains the same.

To model the electron acceleration and $\gamma$-rays emitting in the narrow tube target, 2D-PIC simulations are performed with EPOCH.[18,30,31] During the photon radiation, the emitting electron or positron recoils to maintain the radiation reaction force to be quantum equivalent.[18,30] A 10-PW p-polarized laser pulse with Gaussian spatial and $\sin^2$ temporal profiles, a duration of 30 fs, and a focal spot diameter of 2.0 $\mu$m at FWHM irradiates at a gold narrow tube from the left side. The laser intensity of $3.2 \times 10^{23}$ W/cm$^2$, corresponding to $a_0 \approx 480$, would be available in ELI.[1] The tube $e^-$ (Au$^{+69}$)[32] density is set to $276n_c$ ($4n_c$), where $n_c$ is the critical density. The tube wall, whose thickness is 400 nm and inner diameter is 4 $\mu$m, is located at 2–270 $\mu$m. The simulation box is 271 $\mu$m in the longitudinal direction (x) and 10 $\mu$m in the transverse direction (y). 5 macro-ions and 100 macro-electrons are initialized in each cell whose size is $dx = dy = 5$ nm.

Electron density is transversely modulated by $E_{yL}$, resulting in the generations of high density ($\sim 500n_c$) electron bunches and space charge fields $E_{ys}$ and $E_{xs}$ [Figs. 2(a), 2(d), and 2(e)]. The self-generated field $B_{zs}$[17] [Fig. 2(f)] is generated due to the transport of the electron bunches. The laser fields $E_{xL}$, $E_{yL}$, and $B_{zL}$ and the secondary fields $E_{xs}$, $E_{ys}$, and $B_{zs}$ comprise the fields shown in Fig. 2. Comparison of the locations of the electron bunches, $E_y$ and $E_x$ (Fig. 2), demonstrates that the dragged electrons could be trapped in the acceleration phase of $E_x$, which is consistent with the theory.

In the narrow space, the transverse force $F_\perp$ exerted on the electrons is

$$F_{\perp v} \approx -eE_y + v_x B_z, \tag{3}$$

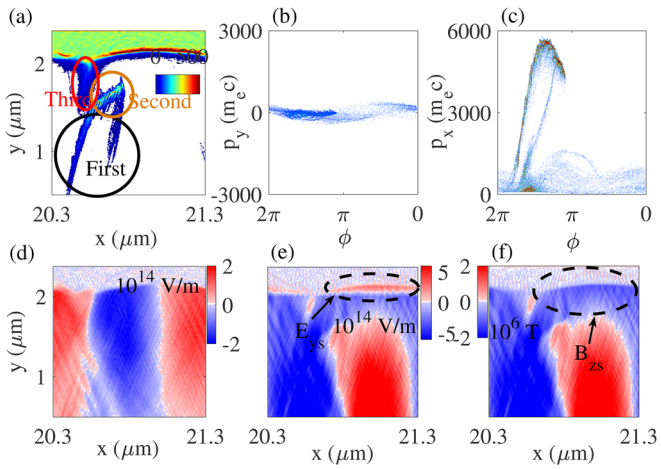


FIG. 2. Simulation results at 100 fs: (a) the electrons pulled into the narrow space can be classified into three groups, the relations between (b) $p_y$, (c) $p_x$, and $\phi$ of the electrons in one bunch and (d) $E_x$, (e) $E_y$, and (f) $B_z$.

where $\vec{E}_y = \vec{E}_{ys} + \vec{E}_{yL}$ and $\vec{B}_z = \vec{B}_{zs} + \vec{B}_{zL}$. By considering the movement process, the dragged electrons can be classified into three groups as shown in Fig. 2(a).

In the first group, the electron movement is dominated by the laser fields as $E_{yL} \gg E_{ys}$ and $B_{zL} \gg B_{zs}$. The electron dynamics can be described by our simple theory. Due to initial large $v_y$, the electrons will cross the laser axis and move toward the other side of the tube where most of the electrons could be trapped again by $E_x$. Hence, the electrons in the first group could be trapped and accelerated by $E_x$ twice. For the electrons in the second group, the high density electron bunch can move with $v_x \approx c$. The self-generated magnetic field of the electrons with high relativistic speed could offset the space charge field in the locality, $E_{ys} \approx cB_{zs}$, which results in $E_y \approx cB_z$ which is also demonstrated in Figs. 2(e) and 2(f). As $F_{\perp v} \to 0$, the electron dynamics follows our theoretical model as well. Thus, the electrons in the second group can be trapped by $E_x$ for a longer time. After crossing the phase of $E_y$, the electrons will be pulled back to the tube wall by $F_{\perp v}$. The electrons in the third group are exposed to larger $E_{ys}$ than $E_{yL}$ as shown in Fig. 2(e). The electrons will be easily pulled back to the tube wall by $E_{ys}$. Thus, the electrons in this group can only contribute to low energy radiation as the acceleration terminates early. The above discussions show that the dynamics of the highly collimated electrons in the NTT is completely different from the regime of laser target direct interaction where the acceleration is dominated by magnetic force or ponderomotive force,[5,9,10,17,26] and the electrons in the first two groups can be phase-locked by $E_x$ for a long time and accelerated effectively.

Figures 3(a) and 3(b) show the fields exerted on an electron in the first group and the second group, respectively. The acceleration of the emitting electron is mostly contributed by the longitudinal field $E_x$ instead of $E_y$ and $B_z$. The laser pulse with a Gaussian profile, which provides the fields for electron acceleration and radiation, can be well maintained up to 300 fs. The emitted electrons can be accelerated to several GeV at a distance $<100\,\mu$m as shown in Figs. 3(c) and 3(d). The two stage acceleration marked in Fig. 3(c) is consistent with the above discussion on the electrons in the first group.

In the tube wall, the direction of $E_y$ turns reversal as circled in Fig. 2(d) and the transverse force $F_\perp$ becomes

$$F_{\perp w} \approx -eE_{ys}\left(1 + \frac{v_x}{c}\right) \approx -2eE_{ys}. \tag{4}$$

From Eqs. (3) and (4), it is found that $F_{\perp w}$ is much larger than $F_{\perp v}$. As discussed above, the electrons will be pulled back to the tube wall, where larger $F_{\perp w}$ will significantly enhance the production of $\gamma$-rays[33] as shown in Figs. 3(e), 3(f), and 4(a).

Figure 4(a) plots the birth positions of the $\gamma$-rays to find out where the $\gamma$-rays are generated. Only half of the tube is plotted to show it clear. One can see that most of the $\gamma$-rays are generated near the inner boundary of the tube. The longitudinal momentum $p_x$ of the emitted photons is much larger than the transverse momentum $p_y$ as shown in Fig. 4(b). The emitting angles of the photons are calculated through $\theta\gamma = \arctan(p_y/p_x)$. After obtaining $\theta\gamma$ of all the photons, a divergence angle of $\sim 2.5^\circ$ is obtained in Fig. 4(c). The forward photons occupy more than 99% of the total generated photons. The characteristics of $\gamma$-rays generated in the NTT are quite different from those of the solid target[5,26] and micro-structured targets.[17,19,20]

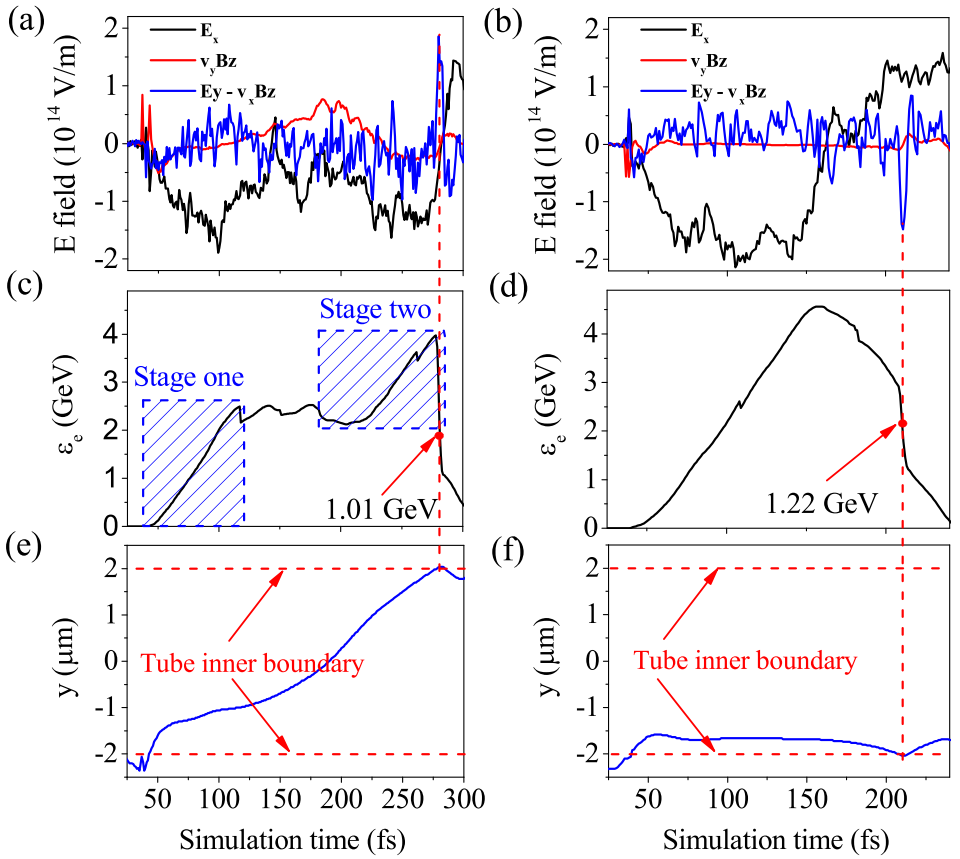


FIG. 3. (a) and (b) The fields exerted on the electron in the first group and the second group, (c) and (d) the kinetic energy history, and (e) and (f) the track of the corresponding emitted electron in the narrow space.

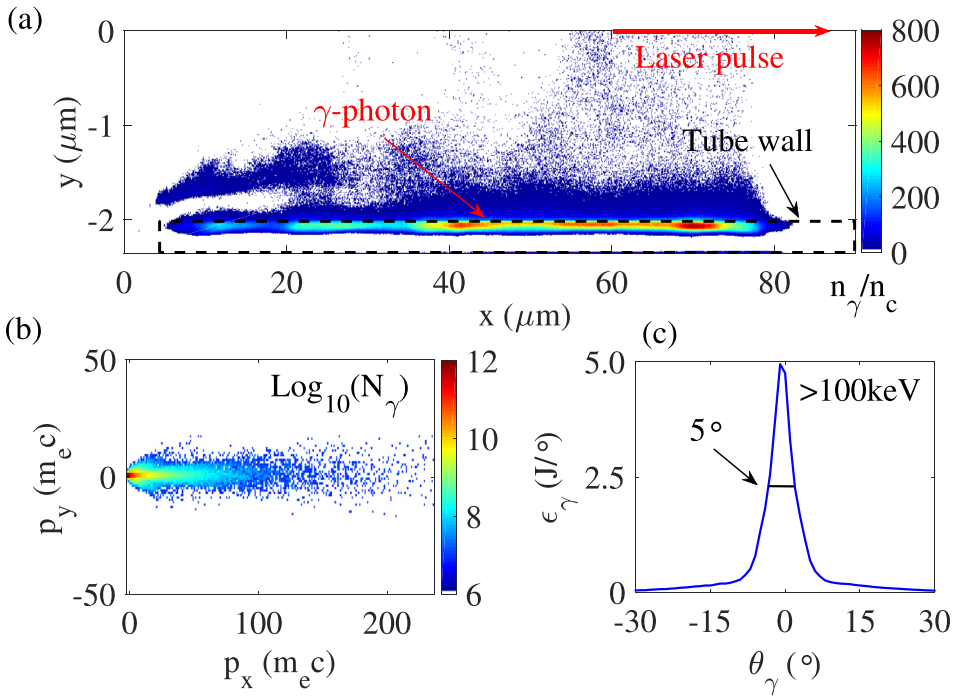


FIG. 4. 2D-PIC simulation results of $\gamma$-ray radiation at 300 fs, showing only the photons with kinetic energy >100 keV. (a) Lower half of the tube showing the relation between the $\gamma$-ray generated positions and the tube wall, the photons are assumed to be at rest after the generations, (b) the phase relation between the longitudinal momentum $p_x(m_e c)$ and transverse momentum $p_y(m_e c)$ of the $\gamma$-ray photons, and (c) the angular distributions of the $\gamma$-ray pulse.

The energy of the emitted $\gamma$-ray photon[18,31] could be estimated as

$$h\nu \approx 0.44\eta\gamma m_e c^2. \tag{5}$$

Here, $\eta \approx \gamma|F_\perp|/(eE_{crit})$. For the generation of energetic $\gamma$-rays, the emitted electrons should be accelerated to high energy before being wiggled as shown in Eq. (5). In the simulation, it is found that the $\gamma$-rays of $\sim$1 GeV can only be generated originally from 18 $\mu$m to 70 $\mu$m as the laser intensity decreases significantly after 70 $\mu$m and most of the photons are generated in 70–200 $\mu$m. The model in the full 3D condition of reduced size 50 $\mu$m NTT is also simulated. It is found that the physical results are almost the same as those in 2D simulation.

In a simulation with a longer run time of 900 fs, only $\sim$10% of the laser energy remains in the simulation window. The simulation time in the rest of this letter is kept at 900 fs which almost covers the whole physics processes. At the end of the simulation, the energy conversion $\eta_\gamma$ ($\eta_e$, $\eta_i$), defined as the total energy transferred from the laser pulse to the forward $\gamma$-rays (electrons, ions), is $\sim$18% ($\sim$61%, $\sim$ 1%). The $\gamma$-ray pulse duration is about 21 fs (6.3 $\mu$m), and the focal spot diameter is about 25 $\mu$m at FWHM. The average photon brilliance is $1.5 \times 10^{25}$ photons/s/mm$^2$/mrad$^2$/0.1%BW at 0.5 MeV, which is two orders higher than the reported results[5,9,10,17,19,26] due to the ultra-small divergence angle and comparable $\eta_\gamma$. It is also found that $\eta_\gamma$, brilliance, and collimation increase with laser intensity $I$, which is consistent with theoretical prediction. The target density in this letter is lower than the solid gold density for the considerations of numerical heating and computational consumption. In a test simulation of the higher density target, the results do not change significantly. To generate highly collimated $\gamma$-ray pulses experimentally using the present method, one can use NTT of much thicker tube wall but the same diameter, as the thickness of the tube does not affect the result. In addition, technical methods are needed to minimize the influence of pre-pulses on the target structure and to inject the laser pulse into the narrow space.

The effects of tube diameter $d$ and laser intensity $I$ on $\theta_\gamma$ and $\eta_\gamma$ are explored to show the robustness of the present mechanism. When $d$ is changed, the laser parameters are fixed. From the expressions of the Gaussian field and $\rho$, one can see that $E_{yL}$ is higher and $\rho$ is smaller in the center. For smaller $d$, more electrons, which contribute to the $\gamma$-ray radiation, are pulled into the vacuum space by larger $E_{yL}$. Hence, $\eta_\gamma$ increases with the decrease in $d$ as shown in Fig. 5(a). Although $\rho$ is proportional to $d$, $E_{yL}$ becomes weaker in the case of larger $d$. Thus, the divergence angle decreases at the beginning and then increases with $d$ decreasing as shown in Fig. 5(a).

In Fig. 5(b), $d$ is fixed to 4$\mu m$ while changing the laser intensity $I$. At higher $I$, the electrons can be accelerated to higher energy and larger $\eta_\gamma$ can be achieved.[27] Hence, $\eta_\gamma$ increases with $I$ and is higher than 31% under $I = 1.28 \times 10^{24}$ W/cm$^2$ as shown in Fig. 5(b). Meanwhile, the $\gamma$-ray pulse is better collimated at higher $I$ because the acceleration in the longitudinal electric field becomes dominant as shown in Fig. 1. At $I = 1.28 \times 10^{24}$ W/cm$^2$, the divergence angle is smaller than 2°.

In conclusion, the electron acceleration of the longitudinal field is illustrated theoretically to resolve the dynamics of

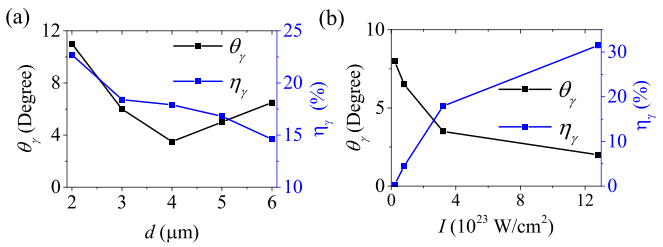


FIG. 5. The effects of tube diameter (a) and laser intensity (b) on the divergence angle of the emitted $\gamma$-ray photon and the energy conversion $\eta_\gamma$ from the laser pulse to the $\gamma$-ray pulse.

energetic electrons in the interaction between an ultra-intense laser and a NTT. Energetic electrons are accelerated efficiently by the longitudinal electric field and radiate strongly near the inner boundary of the tube, resulting in the generation of a highly collimated $\gamma$-ray pulse. The brilliance of the forward $\gamma$-ray pulse, from PIC simulation of the 10-PW laser, is two orders of magnitude higher than the reported results due to high conversion efficiency up to 18% and small divergence angle less than $<3^{\circ}$. This scheme, which paves the way for applications of the laser based high brilliance $\gamma$-ray pulses in the near future, is robust in a wide range of tube diameters and laser intensities.

This work was supported by the National Basic Research Program of China (Grant Nos. 2013CBA01502 and 11475010), NSFC (Grant Nos.11535001 and 11575011), National Grand Instrument Project (Grant No. 2012YQ030142), National Key Research and Development Program of China (Grant No. SQ2016zy04003194), and China Postdoctoral Science Foundation (Grant Nos. 2016M600007 and 2017T100009). The numerical simulations were supported by the Max Planck Computing and Data Facility and the High-performance Computing Platform of Peking University. The PIC code Epoch was in part funded by the UK EPSRC Grants EP/G054950/1.

[1]See www.eli-laser.eu for Extreme light infrastructure project.
[2]See www.xcels.iapras.ru for Exawatt center for extreme light studies.
[3]A. R. Bell and J. G. Kirk, "Possibility of prolific pair production with high-power lasers," Phys. Rev. Lett. **101**, 200403 (2008).
[4]A. Di Piazza, C. Müller, K. Z. Hatsagortsyan, and C. H. Keitel, "Extremely high-intensity laser interactions with fundamental quantum systems," Rev. Mod. Phys. **84**, 1177–1228 (2012).
[5]C. P. Ridgers, C. S. Brady, R. Duclous, J. G. Kirk, K. Bennett, T. D. Arber, A. P. L. Robinson, and A. R. Bell, "Dense electron-positron plasmas and ultraintense $\gamma$ rays from laser-irradiated solids," Phys. Rev. Lett. **108**, 165006 (2012).
[6]Z. Gong, R. H. Hu, Y. R. Shou, B. Qiao, C. Chen, F. Xu, X. He, and X. Yan, "Radiation reaction induced spiral attractors in ultra-intense colliding laser beams," Matter Radiat. Extremes **1**, 308–315 (2016).
[7]J. Schwinger, "On gauge invariance and vacuum polarization," Phys. Rev. **82**, 664–679 (1951).
[8]R. Capdessus, E. d'Humières, and V. T. Tikhonchuk, "Influence of ion mass on laser-energy absorption and synchrotron radiation at ultrahigh laser intensities," Phys. Rev. Lett. **110**, 215003 (2013).
[9]T. Nakamura, J. K. Koga, T. Z. Esirkepov, M. Kando, G. Korn, and S. V. Bulanov, "High-power $\gamma$-ray flash generation in ultraintense laser-plasma interactions," Phys. Rev. Lett. **108**, 195001 (2012).
[10]C. S. Brady, C. P. Ridgers, T. D. Arber, A. R. Bell, and J. G. Kirk, "Laser absorption in relativistically underdense plasmas by synchrotron radiation," Phys. Rev. Lett. **109**, 245006 (2012).
[11]D. L. Burke, R. C. Field, G. Horton-Smith, J. E. Spencer, D. Walz, S. C. Berridge, W. M. Bugg, K. Shmakov, A. W. Weidemann, C. Bula, K. T. McDonald, E. J. Prebys, C. Bamber, S. J. Boege, T. Koffas, T. Kotseroglou, A. C. Melissinos, D. D. Meyerhofer, D. A. Reis, and W. Ragg, "Positron production in multiphoton light-by-light scattering," Phys. Rev. Lett. **79**, 1626–1629 (1997).
[12]O. J. Pike, F. Machenroth, E. G. Hill, and S. J. Rose, "A photon-photon collider in a vacuum hohlraum," Nat. Photonics **8**, 434–436 (2014).
[13]X. Ribeyre, E. d'Humières, O. Jansen, S. Jequier, V. T. Tikhonchuk, and M. Lobet, "Pair creation in collision of $\gamma$-ray beams produced with high-intensity lasers," Phys. Rev. E **93**, 013201 (2016).
[14]X.-L. Zhu, T.-P. Yu, Z.-M. Sheng, Y. Yin, I. C. E. Turcu, and A. Pukhov, "Dense gev electron–positron pairs generated by lasers in near-critical-density plasmas," Nat. Commun. **7**, 13686 (2016).
[15]S. Bulanov, T. Z. Esirkepov, M. Kando, J. Koga, K. Kondo, and G. Korn, "On the problems of relativistic laboratory astrophysics and fundamental physics with super powerful lasers," Plasma Phys. Rep. **41**, 1–51 (2015).
[16]P. Mészáros, "Gamma ray bursts," Astropart. Phys. **43**, 134–141 (2013).
[17]D. Stark, T. Toncian, and A. Arefiev, "Enhanced multi-mev photon emission by a laser-driven electron beam in a self-generated magnetic field," Phys. Rev. Lett. **116**, 185003 (2016).
[18]C. Ridgers, J. G. Kirk, R. Duclous, T. Blackburn, C. Brady, K. Bennett, T. Arber, and A. Bell, "Modelling gamma-ray photon emission and pair production in high-intensity laser–matter interactions," J. Comput. Phys. **260**, 273–285 (2014).
[19]T. Huang, C. Zhou, H. Zhang, S. Wu, B. Qiao, X. He, and S. Ruan, "Collimated gamma photon emission driven by PW laser pulse in a plasma density channel," Appl. Phys. Lett. **110**, 021102 (2017).
[20]L. Yi, A. Pukhov, P. Luu-Thanh, and B. Shen, "Bright x-ray source from a laser-driven microplasma waveguide," Phys. Rev. Lett. **116**, 115001 (2016).
[21]A. P. L. Robinson, A. V. Arefiev, and D. Neely, "Generating "superponderomotive" electrons due to a non-wake-field interaction between a laser pulse and a longitudinal electric field," Phys. Rev. Lett **111**, 065002 (2013).
[22]K. D. Xiao, T. W. Huang, L. B. Ju, R. Li, S. L. Yang, Y. C. Yang, S. Z. Wu, H. Zhang, B. Qiao, S. C. Ruan, C. T. Zhou, and X. T. He, "Energetic electron-bunch generation in a phase-locked longitudinal laser electric field," Phys. Rev. E **93**, 043207 (2016).
[23]J. Yu, W. Zhou, L. Cao, Z. Zhao, L. Cao, L. Shan, D. Liu, X. Jin, B. Li, and Y. Gu, "Enhancement in coupling efficiency from laser to forward hot electrons by conical nanolayered targets," Appl. Phys. Lett. **100**, 204101 (2012).
[24]S. Jiang, L. L. Ji, H. Audesirk, K. M. George, J. Snyder, A. Krygier, P. Poole, C. Willis, R. Daskalova, E. Chowdhury, N. S. Lewis, D. W. Schumacher, A. Pukhov, R. R. Freeman, and K. U. Akli, "Microengineering laser plasma interactions at relativistic intensities," Phys. Rev. Lett. **116**, 085002 (2016).
[25]L. Ji, J. Snyder, A. Pukhov, R. Freeman, and K. Akli, "Towards manipulating relativistic laser pulses with micro-tube plasma lenses," Sci. Rep. **6**, 23256 (2016).
[26]C. S. Brady, C. Ridgers, T. Arber, and A. R. Bell, "Gamma-ray emission in near critical density plasmas," Plasma Phys. Controlled Fusion **55**, 124016 (2013).
[27]C. S. Brady, C. P. Ridgers, T. D. Arber, and A. R. Bell, "Synchrotron radiation, pair production, and longitudinal electron motion during 10-100 PW laser solid interactions," Phys. Plasmas **21**, 033108 (2014).
[28]M. Reiser, *Theory and Design of Charged Particle Beams* (John Wiley & Sons, 2008).
[29]T. P. Wangler, *RF Linear Accelerators* (John Wiley & Sons, 2008).
[30]T. Arber, K. Bennett, C. Brady, A. Lawrence-Douglas, M. Ramsay, N. Sircombe, P. Gillies, R. Evans, H. Schmitz, A. Bell *et al.*, "Contemporary particle-in-cell approach to laser-plasma modelling," Plasma Phys. Controlled Fusion **57**, 113001 (2015).
[31]R. Duclous, J. G. Kirk, and A. Bell, "Monte carlo calculations of pair production in high-intensity laser–plasma interactions," Plasma Phys. Controlled Fusion **53**, 015009 (2010).
[32]B. M. Penetrante and J. N. Bardsley, "Residual energy in plasmas produced by intense subpicosecond lasers," Phys. Rev. A **43**, 3100–3113 (1991).
[33]J. D. Jackson, *Electrodynamics* (Wiley Online Library, 1975).